



Small-angle neutron scattering reveals the effect of Mo on interphase nano-precipitation in Ti-Mo micro-alloyed steels

Y.Q. Wang^{a,b,*}, S.J. Clark^{b,c}, B. Cai^d, D. Alba Venero^e, K. Yan^f, M. Gorley^a, E. Surrey^a, D.G. McCartney^{b,g}, S. Sridhar^h, P.D. Lee^{b,c,**}

^a United Kingdom Atomic Energy Authority, Culham Science Centre, Abingdon OX14 3DB, UK

^b Research Complex at Harwell, Rutherford Appleton Laboratory, Harwell, OX11 0FA Oxfordshire, UK

^c Department of Mechanical Engineering, University College London, Torrington Place, London, WC1E 7JE, UK

^d School of Metallurgy and Materials, University of Birmingham, Birmingham, UK

^e ISIS, STFC Rutherford Appleton Laboratory, Didcot, Oxfordshire, OX11 0QX, UK

^f School of Materials, University of Manchester, Manchester, M13 9PL, UK

^g Advanced Materials Group, University of Nottingham, Nottingham NG7 2RD, UK

^h George S. Ansell Department of Metallurgical and Materials Engineering, Colorado School of Mines, Golden, CO 80401, USA

ARTICLE INFO

Article history:

Received 18 June 2019

Received in revised form 13 August 2019

Accepted 14 August 2019

Available online 27 August 2019

Keywords:

Micro-alloyed steel

Interphase precipitation

Small-angle-scattering

ABSTRACT

Ti-containing micro-alloyed steels are often alloyed with molybdenum (Mo) to reduce nano-precipitate coarsening, although the mechanism is still disputed. Using small angle neutron scattering we characterised the precipitate composition and coarsening of Ti-alloyed and Ti-Mo-alloyed steels. The results demonstrate ~25 at.% of Ti is substituted by Mo in the (Ti, Mo)C precipitates, increasing both the precipitate volume percent and average size. Mo alloying did not retard precipitation coarsening, but improved lattice misfit between precipitate and matrix, contributing to better ageing resistance of the Ti-Mo-alloyed steel. This new understanding opens opportunities for designing ageing-resistant micro-alloyed steels with lean alloying elements.

© 2019 Acta Materialia Inc. Published by Elsevier Ltd. All rights reserved.

High-strength low-alloy steels strengthened through the interphase precipitation (IPP) mechanism have seen a revival for automotive industry since the development of the NANOHTEN steel which has tensile strength up to 780 MPa [1]. IPP is the phenomenon that occurs upon the decomposition of austenite in steels containing strong carbide-forming elements (such as Ti, Mo and V) and results in characteristic periodic planes of fine precipitates [2,3]. In low-carbon steel fine MC (M = Ti, Mo or V) IPP are encapsulated within a soft ferritic matrix which is strengthened through the Orowan mechanism [4] yielding a steel with high strength and formability [5].

However, these MC particles can coarsen during hot rolling or subsequent annealing heat treatment, degrading the strength of the materials significantly. One possible solution reported in the literature is the addition of molybdenum (Mo). Funakawa and Seto [6], and later work conducted by others [7–10] found that steels with Mo additions showed that the mechanical properties were retained longer during high-temperature ageing. These studies were compared to the observed

interphase precipitation in Ti-containing (~0.2 wt%) and Ti-Mo-containing (~0.1wt%Ti and ~0.2wt%Mo) low carbon steels with a fixed basic composition ~0.04%C, 1.5%Mn, 0.2%Si in wt%. It can be seen that in these studies, the atomic ratio of Ti:C and (Ti + Mo):C were designed to be ~1:1. The most well-known mechanism for this effect was reported by Jang et al. [8], who used first principles calculations to propose that the Mo only participates during the early stages of precipitation and becomes passive due to the energetic disadvantage during the subsequent growth and coarsening stages. The coarsening of precipitates is mainly controlled by diffusion of Ti atoms, therefore, the replacement of Ti by Mo reduces the Ti concentration in the ferrite matrix, which decelerates the coarsening of (Ti, Mo)C precipitates [6,8]. Moreover, Funakawa et al. [6] observed that a decrease in Ti concentration from 0.2 wt% to ~0.1 wt% without Mo additions in Ti-containing steel results in similar hardness of Ti-Mo-containing one (~0.1wt%Ti and ~0.2wt% Mo). Jang et al., [11] used CALPHAD and diffusion simulations to show that the coarsening rate of TiC in Fe-Ti-C steels (fixed 0.04%C, wt%) can be significantly retarded by decreasing the Ti/C ratio.

However, both the effect of Ti/C ratio and the Mo on the interphase precipitation have not been well examined quantitatively, which leaves a question to the automotive industry whether it is necessary to add Mo into Ti-containing steels. This is due to the widely used techniques such as transmission electron microscopy (TEM) [12,13] and atom probe

* Correspondence to: Y. Wang, United Kingdom Atomic Energy Authority, Culham Science Centre, Abingdon OX14 3DB, UK.

** Correspondence to: P. Lee, Department of Mechanical Engineering, University College London, Torrington Place, London WC1E 7JE, UK.

E-mail addresses: yiqliang.wang@ukaea.uk (Y.Q. Wang), peter.lee@ucl.ac.uk (P.D. Lee).

tomography (APT) [14–18] which have a limited capability to analyse statistically significant numbers of precipitates. The size difference of precipitates in Ti and Ti-Mo steels presented in the literature is so small (typically in the range of 1.6 nm to 10 nm [7–9]) that it is difficult to statistically and accurately investigate the role of Mo with TEM and APT.

The present study utilizes Small-Angle-Neutron-Scattering (SANS) to study the precipitation behaviour of two micro-alloyed steels aged at 650 °C for various times. One steel (Fe-0.079Ti-0.051C-1.63Mn-0.19Si-0.036Al-0.014P-0.006S-0.007N, wt%) contains Ti with a Ti:C atomic ratio of 0.4. The second steel (Fe-0.07Ti-0.2Mo-0.044C-1.58Mn-0.19Si-0.039Al-0.013P-0.005S-0.0046N, wt%) contains Ti and Mo with a (Ti + Mo):C atomic ratio of ~1. The detailed characterization was undertaken using SANS, through analysis of both the nuclear and magnetic signals, giving quantitative insight into the evolution of the average precipitate size, volume percent, and precipitate chemistry in bulk samples, which are key information to uncover the precipitation kinetics and hardening behaviour. The data obtained is averaged over billions of precipitates and provides new insights not available from TEM or APT where only tens to hundreds of precipitates are typically measured.

The alloys were vacuum induction melted, casted and then forged at about 1250 °C followed by air cooling. Pieces $30 \times 10 \times 5 \text{ mm}^3$ were sectioned and heat treated (See Supplementary Fig. S1a). Firstly, the specimens were austenitized in a salt bath at 1250 °C for 300 s to dissolve pre-existing precipitates and water quenched. Secondly, the specimens were austenitized at 950 °C for 120 s (to control the austenite grain size) then transferred directly to a salt bath at 650 °C for periods ranging from 0 to 36 ks and water quenched. Prolonged long-term ageing for a further 144 ks was performed separately. The austenitization temperature of 950 °C and duration of 120 s were selected in order to balance the compromise between the austenite grain size, the minimisation of carbide precipitation in austenite. Interphase precipitates can only form at the advancing austenite/ferrite boundary an therefore, the majority of the Ti, Mo and C must have remained in solution during austenitization. The precipitation-time temperature diagram obtained by Wang et al. [10] shows that the start times of carbide precipitation in Ti-Mo (0.1%Ti-0.2Mo%) micro-alloyed steel exceeds 150 s at 950 °C.

SANS experiments were performed on the SANS2d beamline at the ISIS Pulsed Neutron Source, UK [19]. A magnetic field of 1.5 T was applied to saturate the ferritic matrix which allows the separation of the magnetic and nuclear scattering. Specimens with dimension of $\sim 9 \text{ mm} \times \sim 9 \text{ mm} \times \sim 1 \text{ mm}$ were cut from the heat treated samples for the SANS measurements. The neutron beam size was 8 mm in diameter and the measurement time was set to 60 min. The sample to detector

distance was 4 m which gave scattering vector, q , covered the range of 0.004 to 0.3 \AA^{-1} . To avoid collecting scattering signal from multi-Bragg diffraction, only neutrons with wavelengths, λ , from 4.5 to 16.5 Å were selected for data analysis [20]. One-dimensional nuclear and “nuclear + magnetic” scattering intensity plots, I (intensity) versus q were obtained by partial azimuthal averaging in 30 sectors around the horizontal and vertical axes of the transmitted beam respectively using the software Mantidplot [21].

The microstructures of polished and 2% Nital etched samples were examined using scanning electron microscopy (SEM) via an FEI Quanta 650 FEG-SEM operated at a voltage of 20 kV. Detailed microstructures of the (Ti,Mo)C precipitates were examined using a JEOL 2100 TEM. Thin foil specimens were mechanically polished to $\sim 30 \mu\text{m}$ in thickness followed by ion beam milling to electron transparency. The microhardness (Hv) of ferrite grains in heat treated samples was measured using a microhardness tester with a load of 0.1 kgf. 20 measurements were conducted for each sample.

Fig. 1a shows the mean value of Hv versus age time at 650 °C for both Ti and Ti-Mo containing steels and the error-bar represents one standard deviation. The Ti-Mo containing steels show slightly higher hardness and better ageing-resistance compared to the steel with only Ti additions. As shown in Fig. 1b and c, the γ to α transformation in both steels occurs rapidly and both reached $\sim 90\%$ completion in a similar duration of 60 s. This agrees with the dilatometry results (Supplementary Fig. S1b). Fig. 1b, c, d and e also show that decreasingly small regions of bainite formed during quenching with increasing isothermal holding. Both SEM and dilatometry measurements reveal that Mo has a small effect on the γ to α transformation. Bright field TEM images of the Ti and Ti-Mo containing samples transformed at 650 °C for 36 ks are shown in Figs. 2(e) and (f). In both alloys, characteristic periodic planes of nano-scale precipitates are observed, indicative of interphase precipitation.

Fig. 2 shows the one dimensional nuclear and magnetic SANS data in the form of Iq^2 versus scattering vector (q) (left hand axis) for the selected isothermally transformed (60 s, 36 ks and 180 ks) alloys. The results for the water quenched sample and the remaining isothermally transformed (0.3 ks, 3.6 ks and 18 ks) samples are shown in Supplementary Figs. S2 and S3. The ratio of magnetic scattering ($I_{mag}(q)$) to nuclear scattering ($I_{nuc}(q)$) intensity, $R(q)$, which is related to the precipitate composition, is shown on the left-hand axis. If all precipitates have the same composition then the value of $R(q)$ would be constant. On the other hand, $R(q)$ would vary if either there were more than one type of precipitate present of differing size or the precipitate composition is size dependent [22]. Clearly, there were two types of particles with significant difference in both size and composition formed in both steels revealed by two different $R(q)$ values of ~ 3 and ~ 1 at low

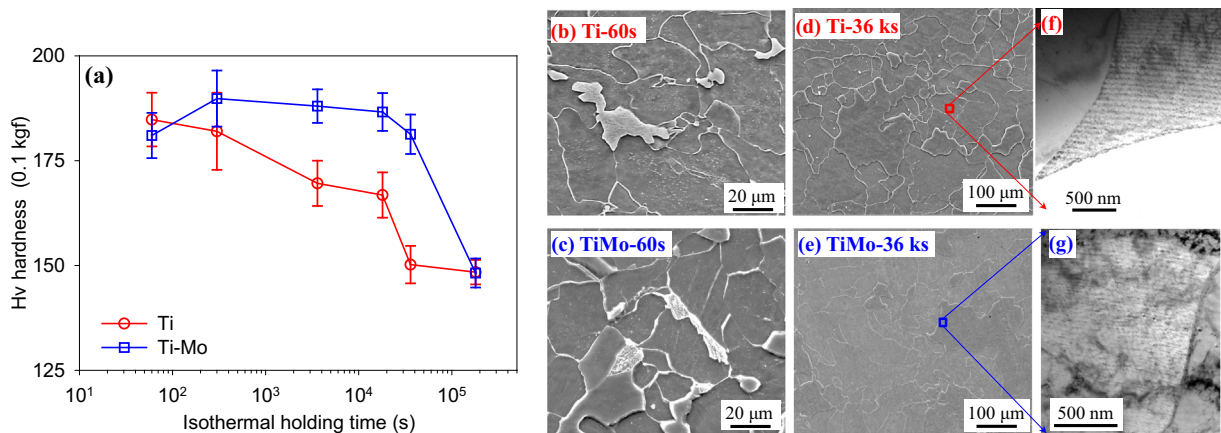


Fig. 1. (a) Effect of isothermal holding time, t , on measured microhardness, Hv, of the Ti and Ti-Mo steels held at 650 °C. Error bars in Hv correspond to one standard deviation from the mean. (b) to (e) SEM images of the Ti (b and c) and TiMo (d and e) samples isothermally transformed for 60 s and 36 ks. (f) and (g) Bright field TEM images of the Ti and TiMo steels respectively after ageing for 36 ks showing interphase precipitation.

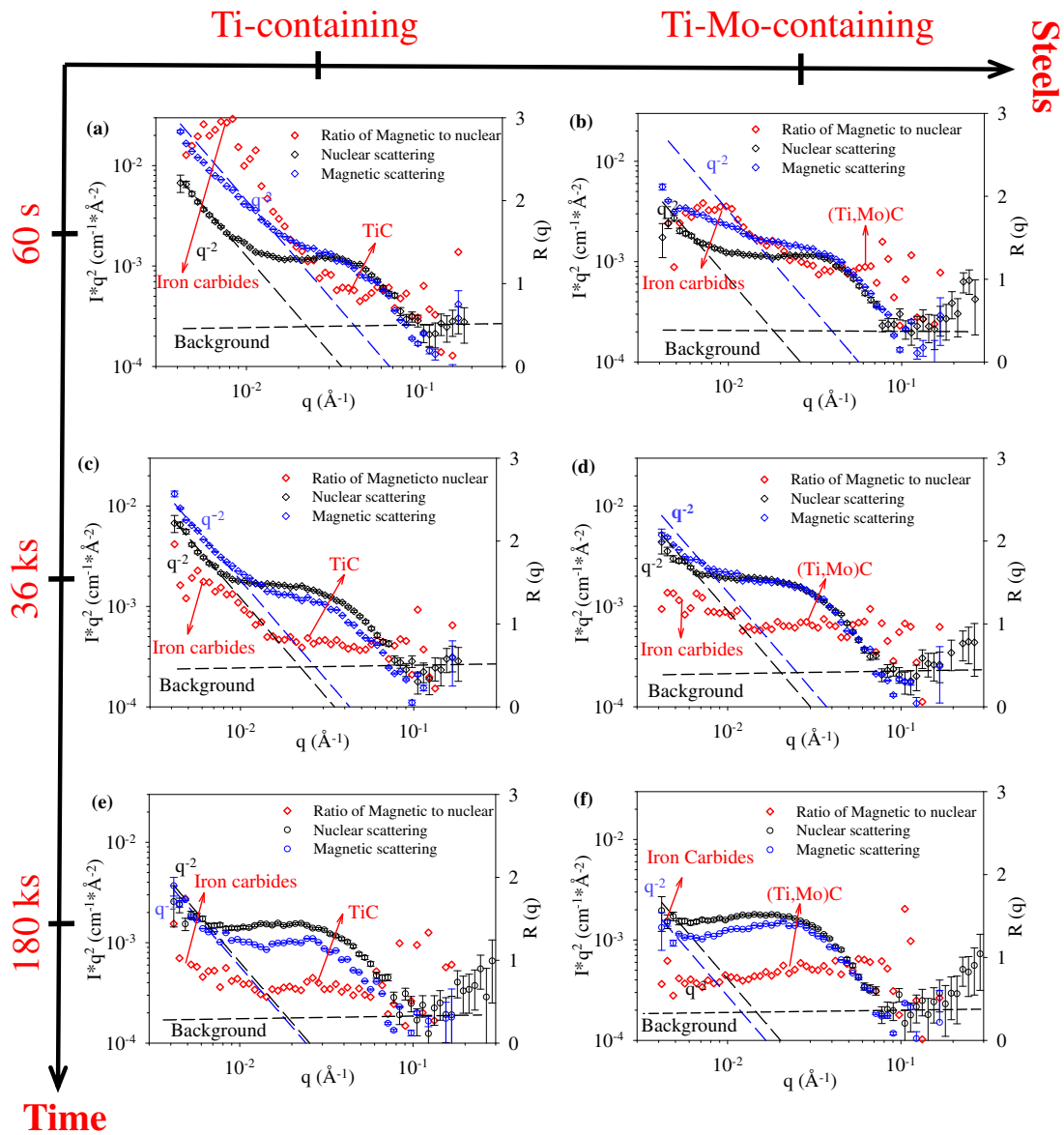


Fig. 2. One-dimensional nuclear and magnetic SANS patterns of Iq^2 (left hand axis) and $R(q)$ (right hand) axis versus scattering vector, q , obtained from the (a, c and e) Ti and (b, d, and f) TiMo samples isothermally transformed at 650 °C for (a and b) 60 s, (c and f) 36 ks, (e and f) 180 ks respectively.

(0.004 to $\sim 0.01 \text{ \AA}^{-1}$) and high (0.02 to $\sim 0.1 \text{ \AA}^{-1}$) q region respectively. A low number density of large ($> 500 \text{ nm}$), cube-shaped TiN precipitates can be formed during casting process and could remain undissolved during the experimental solution treatment [10]. These large TiN precipitates only contribute to the Porod scattering at low q region $< 0.001 \text{ \AA}^{-1}$ and has negligible influence on the scattering signal at q region $> 0.01 \text{ \AA}^{-1}$.

In the low q region, $R(q)$ increases due to the presence of large iron carbides and this is seen to exist in the Ti-containing steels up to 180 ks. In the Ti-Mo containing steels, there is less evidence for an increase in $R(q)$ at low q suggesting less iron carbide forms in this steel. The scattering from large scale iron carbides also reveals itself in the form of a Porod Law slope of approximately q^{-2} on the plot of Iq^2 versus q at the low q region. These large iron carbides (Fig. 1b and c), make only a small contribution to the nuclear scattering signal (because of their small contrast factor) but a significant contribution to the magnetic scattering signal. This causes a marked difference between these two signals at low q as revealed by an increase in the $R(q)$ value. In the samples isothermally held for 180 ks, the matrix phase transformation was

completed so iron carbides did not form following quenching resulting in a smaller difference between the nuclear and magnetic signals across the entire range of q . At high q region, it is the fine IPP that contribute to the nuclear and magnetic signals and so $R(q)$ plateaus from which the chemical composition of the IPP can be estimated. A low number density of large ($> 500 \text{ nm}$), cube-shaped TiN precipitates can be formed during casting process and could remain undissolved during the experimental solution treatment [1]. These large TiN precipitates only contribute to the Porod scattering at low q region $< 0.001 \text{ \AA}^{-1}$ and has negligible influence on the scattering signal at q region $> 0.01 \text{ \AA}^{-1}$.

To isolate the scattering signal only from nano-sized TiC or (Ti, Mo)C precipitates the Porod Law region at low q and the incoherent background in both the nuclear and magnetic SANS signals were subtracted. Fig. 3 shows the mean values of $R(q)$, which were calculated by taking the average of $R(q)$ values in the q range from ~ 0.0194 to $\sim 0.0775 \text{ \AA}^{-1}$ (for samples aged for 60 s to 3.6 ks) and ~ 0.0097 to $\sim 0.0664 \text{ \AA}^{-1}$ (for samples aged from 18 ks to 180 ks). The error in Fig. 3 is given as one standard deviation. The results show that the mean values of $R(q)$ for isothermally transformed Ti and Ti-Mo alloys were ~ 0.70 and ~ 0.95

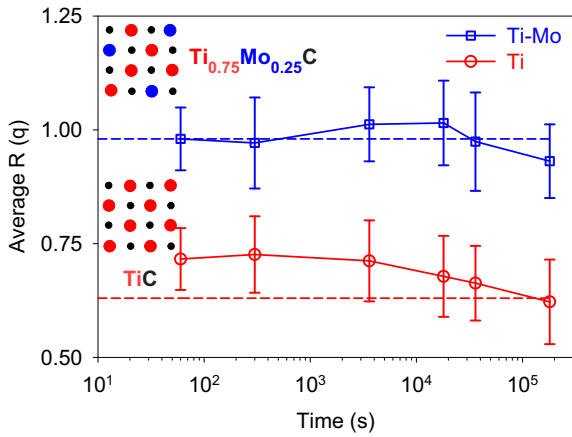


Fig. 3. Plot of the mean value of $R(q)$ as a function of scattering vector, q , calculated from the scattering curves in Fig. 2. $R(q)$ is the ratio of magnetic to nuclear scattering intensity. Theoretical values for TiC and for $\text{Ti}_{0.75}\text{Mo}_{0.25}\text{C}$ are shown by the horizontal lines.

respectively. The ageing time did not change the mean values of $R(q)$ significantly. The theoretical $R(q)$ values of ~ 0.64 and ~ 1 represent the average chemical composition of the precipitates in Ti and Ti-Mo containing steels are TiC and $\text{Ti}_{0.75}\text{Mo}_{0.25}\text{C}$ respectively [21], as shown by the red and blue horizontal lines in Fig. 3. The substitution of Ti with Mo in the precipitates is in excellent agreement with results obtained from APT [18,23–24] and extraction [25] in similar micro-alloyed steels (e.g. 0.05% to 0.2% Ti-0.20%Mo-0.045% C, wt%).

The volume percent (f_v) of TiC and (Ti, Mo)C were calculated from the invariant, Q , of the magnetic SANS signal using the eq. $Q = \int_0^\infty I(q)q^2 dq = 2\pi^2(\rho_p - \rho_m)^2 f_v(1 - f_v)$ [21,26], where ρ_p and ρ_m are the magnetic scattering length densities of precipitate and matrix. The use of magnetic

SANS signal ensures that the volume percent calculation is independent of the chemical composition of the precipitates. Fig. 4a shows that the volume percent of TiC in Ti steels and (Ti, Mo)C in TiMo steels were $\sim 0.10\%$ and $\sim 0.13\%$ respectively and invariant with isothermal holding. The equilibrium volume percent of 0.156 vol% (TiC phase fraction) and 0.157 vol% ((Ti, Mo)C phase fraction) at 650 °C calculated using Thermo-Calc and the TCFE7 database. In the Ti-Mo steel, the equilibrium atomic ratio of Ti to Mo in (Ti, Mo)C precipitates is predicted to be $\sim 9:1$, which indicates the Mo is not strong stabiliser for MC-type carbide.

Fig. 4b, c and d show the Kratky radius (R_{max}), Guinier radius (R) and thickness (T) (disk morphology [24]) of particles obtained from both nuclear and magnetic SANS scattering signs. The Kratky radius is calculated by $R_{max} = \sqrt{3}/q_{max}$ (the “pseudo-Guinier radius”), where the q_{max} determined from the the Kratky plot (Iq^2 vs q) [27]. Alternatively, a radius of gyration, R_{g1} , is extracted from the Guinier plot (which takes the form of $\ln(I)$ vs q^2) using a self-consistent method with $1 < qR_{g1} < 2$. Considering a distribution of monodisperse thin discs of thickness, T , and radius, R , the relationship between T , R and R_{g1} is given by $R_{g1}^2 = T^2/12 + R^2/2$ [28]. A second Guinier plot of $\ln[q^2(I)]$ vs q^2 is known to give a radius of gyration, R_{g2} , that is related to the disc thickness, $R_{g2} = (T^2/12)^{0.5}$. Fig. 4b shows that the average size of the TiC and (Ti, Mo)C interphase precipitates increased from ~ 6.5 nm after 60s to ~ 10 nm after 3.6 ks, but exhibit minimal growth during the further ageing up to 180 ks at 650 °C. The average Guinier radius (Fig. 4c) of disk precipitates has been found ~ 2 nm smaller than Kratky radius, but followed very similar tendency as kratkey radius. Fig. 4d indicated that the average Guinier thicknesses of TiC and (Ti,Mo)C were ~ 5.5 nm and ~ 6.5 nm respectively and both exhibit insignificant evolution (< 1.5 nm) during isothermal ageing. Hence, the hypothesis that the Mo can retard the growth and coarsening of (Ti,Mo)C interphase precipitation is not supported by our results, which show the average precipitate size in aged Ti-containing steels were even slightly smaller than in aged Ti-Mo-containing steels.

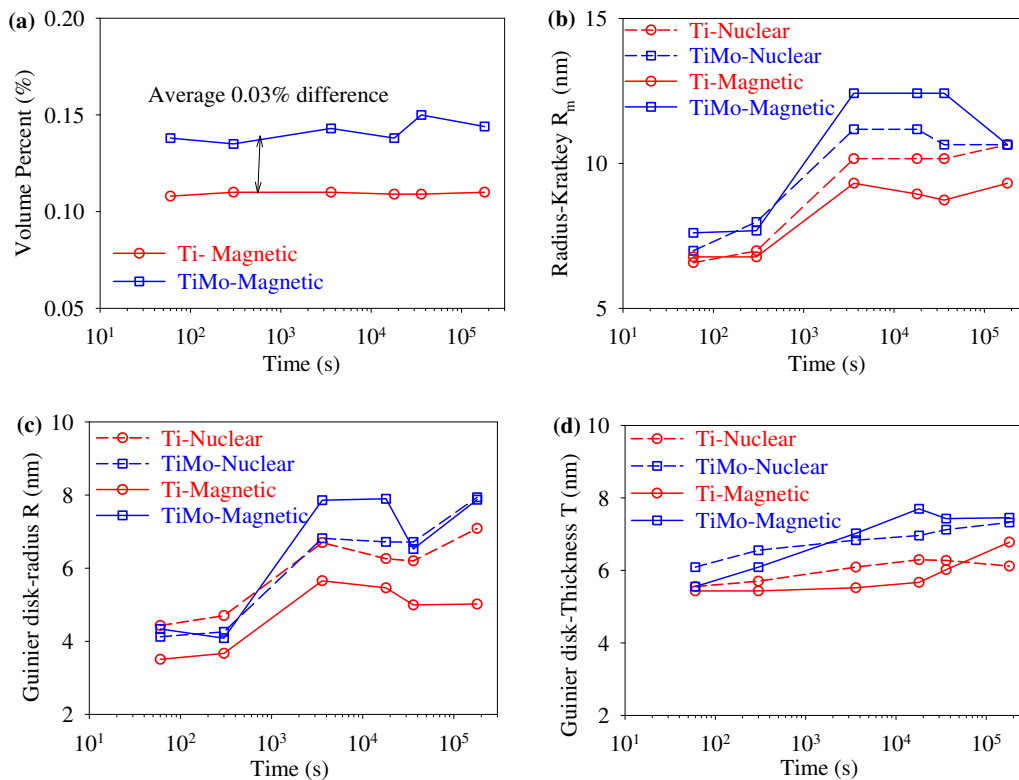


Fig. 4. Graphs to show the effect of isothermal holding time, t on carbide particle volume fraction and particle dimensions in Ti and TiMo alloys aged at 650 °C. (a) Particle volume percent calculated from analysis of the invariant, Q , of the magnetic SANS data. Particle dimensions obtained from (b) Kratky radius, R_{max} , assuming spherical-shaped particles and (c) and (d) Guinier analysis assuming disk-shaped particles. (c) shows the disk radius, R , versus ageing time, t , and (d) shows disk thickness, T , versus time, t .

The precipitates coarsening rates in both alloys were extremely low. In Ti-containing steels it is known that a low Ti/C ratio (0.4) causes the concentration of Ti at the precipitate-ferrite interface to become small and therefore the diffusion gradients which drive coarsening become shallow and slow [11]. While in Ti-Mo added steels, although the $Ti + Mo/C = 1$ and Mo incorporated into the precipitates at nucleation, the subsequent growth of precipitates is controlled by the diffusion of Ti atoms rather than Mo. We can conclude that the addition of Mo slightly improved the ageing-resistance of the steels (Fig. 1a) is due to (Ti,Mo)C having a reduced misfit strain between the carbide and ferrite matrix than TiC [8,29], rather than Mo retarding coarsening of the precipitates. Seol et al. [30] and Wang et al. [31–32] indicated that Mo can segregate at precipitate's outer to form a core-shell structure with Ti-rich core and Mo-rich shell. Mo layer inhibits the diffusion of Ti, and V from the matrix into the precipitates, which impedes particle coarsening. Whether this mechanism exists in Ti-Mo added steels needs future investigation. The current work only shows the Mo did not retard the global growth and coarsening of (Ti,Mo)C in 0.07%Ti-0.2%Mo (wt%) micro-alloyed steels.

The addition of Mo also slightly increased the hardness of the steels (Fig. 1a). This is due to the higher volume percent of interphase precipitates rather than a decreased average size of precipitate. Approximately 25 at.% Mo co-precipitates as (Mo,Ti)C at the early stage of precipitation and this increased the volume percent of these precipitates from ~0.1% to ~0.13%. This yields ~7% improvement in the precipitation strengthening effect based on the Ashby-Orowan equation

$$\Delta\sigma_{ppt} = \frac{0.538Gb_f^{0.5}}{2R} \ln\left(\frac{R}{b}\right)$$
 [9,33,34]. Where, $\Delta\sigma_{ppt}$ is the increase in yield strength, G is the shear modulus, b is the Burgers vector, f_v is the carbide volume fraction and R is the mean carbide radius.

In summary, our SANS results (nuclear and magnetic scattering signals) reveal Mo does not play a role in retarding nano-precipitate coarsening, which is in contrary to existing literature. Instead, our results show that approximately 25 at.% Mo replaced Ti in the (Mo,Ti)C precipitates, increasing both the precipitate volume percent and average size, and changing the lattice spacing, altering the coherency. Ti-Mo-alloyed steel has higher volume fraction of nano-precipitates than Ti-alloyed steel hence higher hardness. The better ageing-resistance of the Ti-Mo steels than Ti only steels is mainly due to the decrease in misfit between the carbide and matrix leading to coherency being maintained at longer ageing times in Ti-Mo alloyed steel. This new understanding opens opportunities for design of ageing-resistant micro-alloyed steels with significantly less amount of Mo.

Acknowledgements

The authors are thankful to Dr. Arjan Rijkenberg from Tata Steel for providing the experimental materials. This work was made possible via funding from the EPSRC (grants EP/L018705/1, EP/L018632/1 and

EP/M009688/1), and the facilities and support provided by the Research Complex at Harwell. The authors gratefully acknowledge the use of the SANS2D beamline at ISIS Neutron Source (RB1620206). Dr. Wang, Dr. Gorley and Dr. Surrey would also like to acknowledge the RCUK Energy Programme under grant EP/T012250/1 and the UK Government Department for Business, Energy and Industrial Strategy.

References

- [1] Y. Funakawa, T. Shiozaki, K. Tomita, T. Yamamoto, E. Maeda, *ISIJ Int.* 44 (11) (2004) 1945–1951.
- [2] A. Davenport, F. Berry, R. Honeycombe, *Metal Sci.* 2 (1) (1968) 104–106.
- [3] S.-P. Tsai, Y.-T. Tsai, Y.-W. Chen, J.-R. Yang, C.-Y. Chen, Y.-T. Wang, C.-Y. Huang, *Scr. Mater.* 143 (2018) 103–107.
- [4] T. Gladman, *Maney Pub*, 1997.
- [5] F. Yoshimsa, F. Takeshi, Y. Katsumi, *J.F.E. Tech. Rep. No.* (2013) 18.
- [6] Y. Funakawa, K. Seto, *Tetsu-to-Hagane*. 93 (1) (2007) 49–56.
- [7] C. Chen, H. Yen, F. Kao, W. Li, C. Huang, J. Yang, S. Wang, *Mater. Sci. Eng. A*. 499 (1) (2009) 162–166.
- [8] J.H. Jang, C.-H. Lee, Y.-U. Heo, D.-W. Suh, *Acta Mater.* 60 (1) (2012) 208–217.
- [9] N. Kamikawa, Y. Abe, G. Miyamoto, Y. Funakawa, T. Furuhashi, *ISIJ Int.* 54 (1) (2014) 212–221.
- [10] Z. Wang, H. Zhang, C. Guo, W. Liu, Z. Yang, X. Sun, Z. Zhang, F. Jiang, *J. Mater. Sci.* 51 (10) (2016) 4996–5007.
- [11] J. Jang, C. Lee, H. Han, H. Bhadeshia, D. Suh, *Mater. Sci. Technol.* 29 (9) (2013) 1074–1079.
- [12] H.-W. Yen, P.-Y. Chen, C.-Y. Huang, J.-R. Yang, *Acta Mater.* 59 (16) (2011) 6264–6274.
- [13] H.-W. Yen, C.-Y. Huang, J.-R. Yang, *Scripta Mater.* 61 (6) (2009) 616–619.
- [14] Y.-J. Zhang, G. Miyamoto, K. Shinbo, T. Furuhashi, *Scr. Mater.* 69 (1) (2013) 17–20.
- [15] Y. Kobayashi, J. Takahashi, K. Kawakami, *Scr. Mater.* 67 (10) (2012) 854–857.
- [16] I. Timokhina, P. Hodgson, S. Ringer, R. Zheng, E. Pereloma, *Scr. Mater.* 56 (7) (2007) 601–604.
- [17] C. Enloe, K. Findley, C.M. Parish, M.K. Miller, B. De Cooman, J. Speer, *Scr. Mater.* 68 (1) (2013) 55–58.
- [18] J. Wang, M. Weyland, I. Bikmukhametov, M.K. Miller, P.D. Hodgson, I. Timokhina, *Scr. Mater.* 160 (2019) 53–57.
- [19] R. Heenan, S. Rogers, D. Turner, A. Terry, J. Treadgold, S. King, *Neutron News* 22 (2) (2011) 19–21.
- [20] A. Michels, J. Weissmüller, *Rep. Prog. Phys.* 71 (6) (2008), 066501.
- [21] Y. Wang, S. Clark, V. Janik, R. Heenan, D.A. Venero, K. Yan, D. McCartney, S. Sridhar, P. Lee, *Acta Mater.* 145 (2018) 84–96.
- [22] B.S. Seong, E. Shin, S.-H. Choi, Y. Choi, Y.S. Han, K.H. Lee, Y. Tomota, *Appl. Phys. A* 99 (3) (2010) 613–620.
- [23] I. Bikmukhametov, H. Beladi, J. Wang, P.D. Hodgson, I. Timokhina, *Acta Mater.* 170 (2019) 75–86.
- [24] S. Mukherjee, I. Timokhina, C. Zhu, S. Ringer, P. Hodgson, *Acta Mater.* 61 (7) (2013) 2521–2530.
- [25] Y. Tanaka, S. Kinoshiro, H. Nakamichi, *JFE Tech. Rep. No.* 37 (2016) 31–36.
- [26] F. De Geuser, A. Deschamps, *C R Phys* 13 (3) (2012) 246–256.
- [27] A. Deschamps, F. De Geuser, *J. Appl. Crystallogr.* 44 (2) (2011) 343–352.
- [28] H. Yasuhara, K. Sato, Y. Toji, M. Ohnuma, J. SUZUKI, Y. Tomota, *Tetsu-to-Hagane*. 96 (9) (2010) 545–549.
- [29] J. Jang, Y. Heo, C. Lee, H. Bhadeshia, D.-W. Suh, *Mater. Sci. Technol.* 29 (3) (2013) 309–313.
- [30] Z. Wang, H. Chen, Z. Yang, F. Jiang, *Mater. Trans. A* 49 (5) (2018) 1455–1459.
- [31] Z. Wang, X. Sun, Z. Yang, Q. Yong, C. Zhang, Z. Li, Y. Weng, *Mater. Sci. Eng. A*. 573 (2013) 84–91.
- [32] J.B. Seol, S.H. Na, B. Gault, J.E. Kim, J.C. Han, C.G. Park, D. Rabbe, *Sci. Rep.* 7 (2017) 42547.
- [33] M.-Y. Chen, M. Gouné, M. Verdier, Y. Bréchet, J.-R. Yang, *Acta Mater.* 64 (2014) 78–92.
- [34] P. Gong, X. Liu, A. Rijkenberg, W. Rainforth, *Acta Mater.* 161 (2018) 374–387.